Journal of Hazardous Materials 415 (2021) 125660

Contents lists available at ScienceDirect

Journal of Hazardous Materials

journal homepage: www.elsevier.com/locate/jhazmat

Structural properties of deprotonated naphthenic acids immersed in water in pristine and hydroxylated carbon nanopores from molecular perspectives

Mingshan Zhang, Wenhui Li, Zhehui Jin *

School of Mining and Petroleum Engineering, Department of Civil and Environmental Engineering, University of Alberta, Edmonton, AB T6G 1H9, Canada

ARTICLE INFO

Editor: Dr. T. Meiping

Keywords:
Naphthenic acids
Interface water
Activated carbon nanopores
Adsorption
Molecular dynamics simulations

ABSTRACT

We use molecular dynamic simulations to study the structural properties of deprotonated cyclohexanoic acid (DCHA) and heptanoic acid (DHA) immersed in water in pristine and hydroxylated carbon nanopores (PACNs and HACNs) in relation to NA removal by activated carbons (ACs). In PACNs, both NAs can aggregate on the pore surface by depleting water molecules, while water molecules accumulate in the area where there is no NA aggregation. The hydrophobic tails of NAs are generally in the interface water region (IWR), while the hydrophilic head groups prefer to be hydrated by water and form pairing with Na^+ ions outside the IWR. The linear carbon tails of DHA tend to be parallel to the pore surface, while a slightly inclined configuration of the carbon ring in DCHA is observed. In HACNs, water forms a predominant interface layer by forming hydrogen bonding with -OH groups, while the hydrophobic tails of NAs are driven away from the surface. Both NAs have a more perpendicular orientation close to the pore surface with their hydrophilic head groups forming hydrogen bonding with -OH groups. The strong water film greatly reduces hydrophobic interactions as well as decreases the available adsorption sites for NAs.

1. Introduction

Nowadays, the bitumen deposits in the Athabasca oil sands region (AOSR) are mainly recovered by surface mining process, during which a vast amount of steam is injected into the formations (Stringham, 2012; A.E. Regulator, 2018). The oil sands process-affected water (OSPW) from the bitumen extraction process may result in a number of environmental concerns, such as acute and chronic toxicity affecting aquatic and mammalian species (Frank et al., 2008). OSPW consists of complex mixtures of organic and inorganic constituents, among which, naphthenic acids (NAs) are the primary toxic components. NAs are mixtures consisting of saturated aliphatic and alicyclic carboxylic acids, mostly containing 2 or 3 rings with 13–27 carbons in their structures (Frank et al., 2008; Wang et al., 2013). The polar carboxylic groups and the non-polar aliphatic ends result in amphiphilic characteristics. In practices, the caustic hot water separation process results in alkaline conditions of OSPW (Allen, 2008), during which NAs are generally deprotonated as naphthenates. NAs can also cause severe corrosions in extraction equipment, pipelines, and storage tanks, increasing operational costs (Slavcheva et al., 1999). Therefore, it is imperative to remove NAs from OSPW to make oil sands operations more environmentally and economically sustainable.

Organic pollutants removal by adsorption in various carbonaceous materials has been developed during the past decades (Yang et al., 2021; Zhu et al., 2021). NA adsorption from water in activated carbons (ACs) is a cost-effective and efficient method to remove NAs (Islam et al., 2018; El-Din et al., 2011), thanks to their high specific surface area arising from the well-developed internal micro- and meso-porous structures (Yuan et al., 2010). It is well known that slit-shaped pores with sizes in the range of a few to hundreds of angstroms are widely distributed in ACs (Choma and Jaroniec, 2006; Sing, 1985). The high-surface-area ACs can effectively adsorb NAs from OSPW to increase their concentrations to trigger specific microbial metabolism mechanisms to preferably accelerate compound-specific biodegradations (Islam et al., 2015). Various O- and N-containing functional groups might be introduced onto the AC surfaces through activation processes or surface modification techniques (Allen et al., 1998; Qiao et al., 2010). However, there have been a limited number of experimental measurements on NA adsorption from water in ACs. They generally proposed that hydrophobic interactions between carbon surface and NAs are the dominant factor for NA adsorption from water in ACs (Bhuiyan et al., 2017; Niasar et al., 2016; Wu and Pendleton, 2001). In addition, NAs with

* Corresponding author.
E-mail address: zhehui2@ualberta.ca (Z. Jin).

https://doi.org/10.1016/j.jhazmat.2021.125660
Received 16 August 2020; Received in revised form 10 March 2021; Accepted 11 March 2021
Available online 18 March 2021

linear-chain structures are reported to be preferentially removed compared to those with cyclic-ring structures (Alam et al., 2016; Zubot et al., 2012) due to the stronger hydrophobicity of linear carbon chains. O-containing functional groups on carbon surfaces generally have an adverse effect on the adsorption capacity of saturated fatty acids and aromatic compounds from water in ACs due to the formation of water clustering around surface groups (Wu and Pendleton, 2001; Pendleton et al., 2002; El-Sayed and Bandosz, 2003). Recently, there have been a number of experimental studies reporting that the formation of the negatively charged assisted hydrogen bond, (-)CAHB between weak acid and carbon surface O-containing groups, especially when they have a similar acidity (i.e., similar pKa values), can increase the adsorption of weak acids on negatively charged carbonaceous surfaces (Moustafa et al., 2014; Li et al., 2015, 2013).

While these experimental measurements proved the efficacy of ACs in NA removal from water, the proposed mechanisms remain as hypotheses and the observation is on the macroscopic scale (such as adsorption capacity). The structural properties of NAs and water cannot be revealed from these experimental measurements, which plays an important role in the underlying mechanism of NA adsorption from water in ACs. However, the pores in ACs are generally in the nanometer scale (Quinlivan et al., 2005), while the structural and thermodynamic properties of NAs immersed in water in ACs are determined by NA-water-surface interactions and individual molecular configurations (linear/cyclic NAs and their distinct structures) which are at the microscopic scale. It has been shown that the interface water structures play an important role in substrate properties (Ali et al., 2020; Li et al., 2020), which can greatly influence the solute-surface interactions. While Ma and Chen (2016) investigated the adsorption properties of cyclohexane carboxylic acids on four-nitrogen coordinated embedded graphene (TMN4-G) by the first-principle density functional theory (DFT), their study focuses on the direct interaction between NAs and carbon surface, while water is not included in their model. Therefore, it is necessary to study structural properties of NAs and interface water structures in different AC nanopores to reveal the effect of NA types (with/without rings) and surface functional groups from molecular scale to provide important insights into NA adsorption mechanism and carbonaceous adsorbents design.

In this work, we use molecular dynamics (MD) simulations to explicitly study the NA-water-surface interactions and individual molecular configurations (with/without rings) to reveal the effect of NA types and O-containing functional groups (represented by -OH group, which is one of most common functional groups) on the structural and thermodynamic properties of NAs and interface water structures in relation to NA removal from water in AC nanopores. While experimental measurements have difficulties in revealing the microscopic scale physical phenomena, MD simulations can explicitly consider the intermolecular interactions and individual molecule as well as surface characteristics from atomistic and molecular perspectives. We use deprotonated heptanoic acid (DHA; chemical formula: $C_7H_{13}O_2^-$) with a linear hydrophobic tail structure and deprotonated cyclohexanecarboxylic acid (DCHA; chemical formula: $C_7H_{11}O_2^-$) with a ring hydrophobic tail structure to represent two different NAs, as the pKa values of cyclohexanecarboxylic acid (4.91) and heptanoic acid (4.8) are lower than the typical pH values in OSPW (pH 8 $\pm$ 0.7) (Moustafa et al., 2014). While these NAs are generally lighter than the ones observed in OSPW (Frank et al., 2008; Wang et al., 2013), as they have amphiphilic characteristics (hydrophilic heads and hydrophobic tails), their structural properties can reveal underlying mechanisms about NA adsorption from water in ACs and the effect of hydrophobic tails. We note that as the pKa value of -OH groups grafted on carbon surface is generally around 10 (Orth et al., 2016), which is above the typical pH value of OSPW, the fully protonated -OH groups are applied, while the formation of (-)CAHB is not considered in this work. We find that in pristine AC nanopores (PACNs), both NAs can aggregate on the pore surface by depleting water molecules, while water accumulate close to the pore surface due to entropic effect (Thomas and McGaughey, 2009) where there is no DHA/DCHA aggregation. The hydrophobic tails of NAs are generally within the interface water region (IWR), especially for DHA, while the hydrophilic head groups are outside the IWR to be better hydrated by water and form pairing with Na^+ ions. On the other hand, in hydroxylated AC nanopores (HACNs), there is a predominant interface water layer thanks to the hydrogen bond (H-bond) between water and -OH groups, while both DHA and DCHA molecules are repelled from the surface. Water forms clustering around -OH groups via the H-bond, while NAs can also form the H-bond with -OH groups by depleting a small number of water molecules. In contrast to PACNs, only hydrophilic head groups of NAs are within the IWR, while their hydrophobic tails are outside the IWR. The drastically different interface water structures in PACNs and HACNs are responsible for the different NA structural properties. Collectively, our work provides important insights into NA structural properties immersed in water in AC nanopores and the optimization of high-performance carbonaceous materials for OSPW remediation.

2. Molecular model and simulations

The molecular structures of DCHA and DHA are shown in Fig. 1. The log K_{ow} of non-deprotonated cyclohexanecarboxylic acid and heptanoic acid are 2.36 and 2.54, respectively, while those of DCHA and DHA are -1.71 and -1.06, respectively (Moustafa et al., 2014), demonstrating a much stronger hydrophilicity for the deprotonated ones. In addition, both of the non-deprotonated and deprotonated heptanoic acids are more hydrophobic than the corresponding cyclohexanecarboxylic acids. Na^+ ions are used as the counter-ions in this work. As a typical O-containing functional group, hydroxyl (-OH) groups which commonly appear on the AC surfaces during the activation process (Oda et al., 2006) are grafted on carbon surface to study their effect. We use carbon slit pores with each substrate consisting of three graphene layers to represent PACNs. On the other hand, for HACNs, -OH groups are evenly grafted onto the both carbon substrates with the oxidation degree $D = N_O/N_C$ (N_O and N_C are the number of O atoms and C atoms in the same layer, respectively) as 0.125, which is a typical oxidation value for O-containing functional groups on AC surfaces (Müller and Gubbins, 1998; Figueiredo et al., 1999), as depicted in Fig. 2. While a random patterned -OH group distribution commonly occurs in AC nanopores, for simplicity, we use a regular patterned one to investigate the effect of -OH groups on the structural properties of NAs and water in HACNs. A rectangular-cuboid-shaped simulation box with a dimension of $L_X =$ 5.904 nm and $L_Y = 5.965$ nm in the X- and Y-directions, respectively, is used. To minimize the influence from the periodic images in the Z-direction, a vacuum is placed in the simulation cell with a length much larger than L_X or L_Y in the Z-direction (Alejandre et al., 1995). As a result, the box size in the Z-direction L_Z is determined by pore size and the vacuum length. The pore size W is defined as the separation distance between the carbon atoms on the innermost planes of the two graphene layers in the Z-direction. We use $W = 1.5$ nm and $W = 4$ nm to represent micropores and mesopores, respectively (Rouquerol et al., 1994), which can represent typical nanopores in ACs (Pelekani and Snoeyink, 1999). The molecular models, force fields and simulation details are provided in Supporting Information (SI).

3. Results and discussion

3.1. PACNs

In Fig. 3, we present the schematic representations of the equilibrated systems with DCHA and DHA, Na^+ ions as well as water molecules in PACNs. In pristine AC micropores, both DCHA and DHA tend to stay close to the pore surface with their hydrophobic tails attached to the pore surface, while their hydrophilic heads point toward the middle of the pores. However, they reveal distinct conformational characteristics

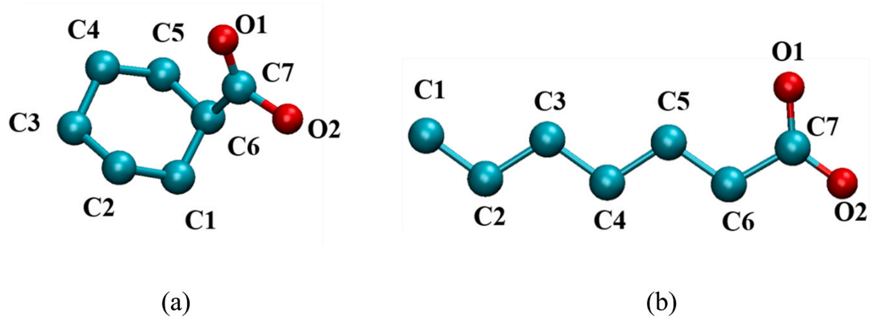

Fig. 1. Molecular structures of (a) DCHA; (b) DHA. Color scheme: red, O; cyan, C. The H atoms are not shown here for clarity. (For interpretation of the references to color in this figure legend, the reader is referred to the web version of this article.)

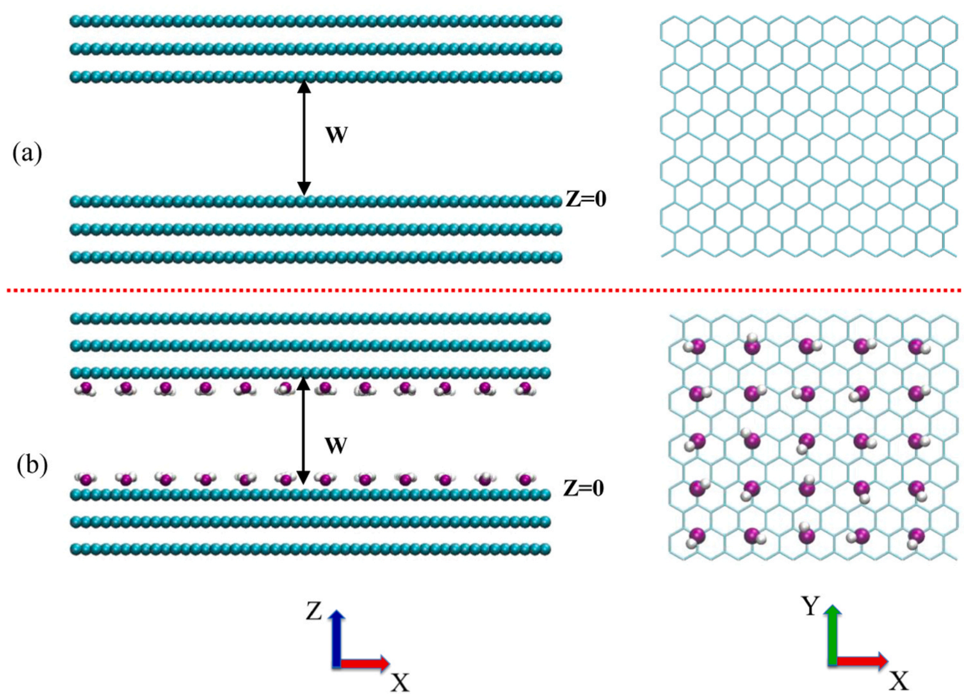

Fig. 2. Schematic representations of (a) PACNs; (b) HACNs. Color scheme: white, H; purple, O of -OH groups; cyan, C. (For interpretation of the references to color in this figure legend, the reader is referred to the web version of this article.)

owing to different molecular structures. The linear hydrophobic tails of DHA incline to be parallel to the surface thanks to the strong hydrophobic interaction between aliphatic chains and the carbon surface in line with previous studies (da Silva and Miranda, 2013; El-Sayed and Bandosz, 2004). On the other hand, a slightly inclined configuration of the carbon ring in DCHA is observed due to the entropy loss arising from the ring structure close to the pore surface (Alam et al., 2016; Spitzer and Heerze, 1983). Similar configurations are also observed in mesopores. The differences in the structural properties of NAs with/without a ring hydrophobic tail structure is probably responsible for their distinct removal behavior (Zubot et al., 2012; Quinlan and Tam, 2015). In mesopores, some DCHA molecules are immersed in water far away from the pore surface, while all DHA molecules are bound to the pore surface. For all cases, Na^+ ions are depleted from the pore surface.

To understand NA configurational properties in the vicinity of the pore surface and interface water structures, in Fig. 4, we present the schematic views of the *X-Y* plane in pristine AC mesopores. For DCHA, the plane view covers the region from $Z = 0$ to $Z = 0.66$ nm, while for DHA, it covers the region from $Z = 0$ to $Z = 0.6$ nm. $Z = 0.66$ nm for DCHA and $Z = 0.6$ nm for DHA correspond to the positions where the C6 number density is close to 0 as shown in Fig. 5. DHA and DCHA molecules can aggregate on the pore surfaces by depleting water molecules, while water molecules accumulate close to the pore surface due to entropic effect (Thomas and McGaughey, 2009; Wu et al., 2011) where there is no DHA/DCHA aggregation. The depletion of water molecules from pristine carbon surface demonstrates the strong hydrophobic interaction between NAs and carbon surfaces. On the other hand, the Na^+ ions tend to be hydrated by water rather than forming pairing with NA molecules. O1 (O2) atoms are mainly hydrated by water, while their pairing with Na^+ ions is insignificant as shown in Table S2 in SI. The hydration and pairing number calculation method can be referred to our previous work (Zhang and Choi, 2006). Similar phenomenon is observed in micropores, which is not shown here.

In Fig. 5, we present the number density distributions of each species in NAs and water oxygen as well as hydrogen (denoted as O_w and H_w, respectively) in pristine AC mesopores. As the O1 and O2 in the deprotonated carboxyl groups are equivalent (Immaraporn et al., 2004), we only show the O1 distributions. Water shows a layering structure close to the pore surface with a strong first adsorption layer due to the entropic effect (Thomas and McGaughey, 2009; Wu et al., 2011), despite carbon surface is generally perceived as hydrophobic (Kozbial et al., 2016). The locations of peaks in the first O_w and H_w adsorption layers

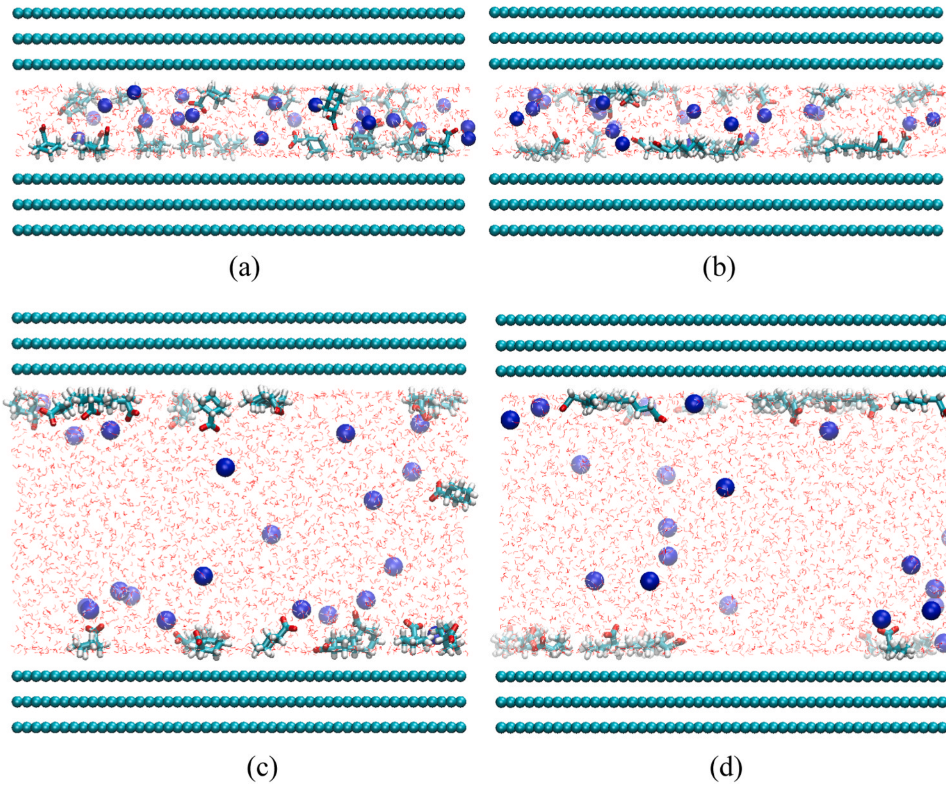

Fig. 3. Schematic representations of (a) DCHA; (b) DHA, Na^+ ions, and water molecules in pristine AC micropores and (c) DCHA; (d) DHA, Na^+ ions, and water molecules in pristine AC mesopores. Color scheme: white, H; red, O; cyan, C, blue Na^+. For clarity, water molecules are presented by the line mode. (For interpretation of the references to color in this figure legend, the reader is referred to the web version of this article.)

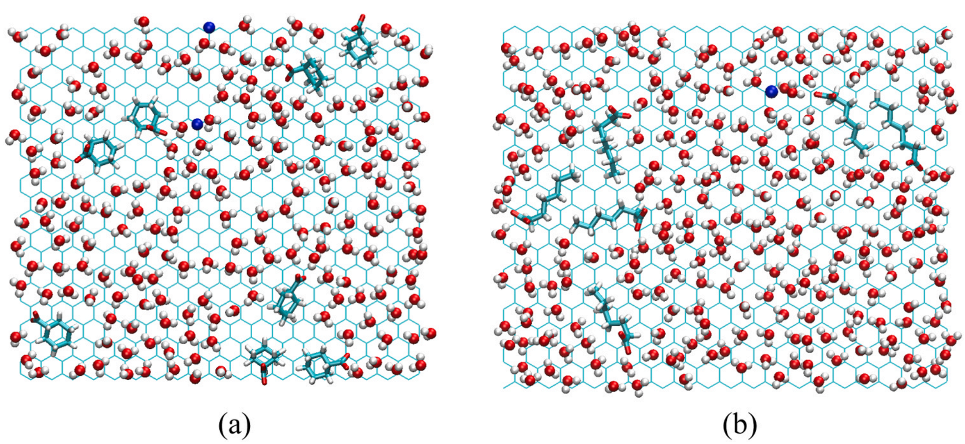

Fig. 4. The schematic view of the *X-Y* plane with (a) DCHA; (b) DHA in pristine AC mesopores. For DCHA, the plane view covers the region from $Z = 0$ to $Z = 0.66$ nm; For DHA, the plane view covers the region from $Z = 0$ to $Z = 0.6$ nm.

coincide, suggesting that interface water molecules tend to orientate parallel to the wall (Ulberg and Gubbins, 1995). Water orientation distributions $S(Z)$ is presented in Fig. S1 in SI, which are given as,

$$S(Z) = 1.5\langle\cos^2\alpha\rangle - 0.5, \tag{1}$$

where α is the angle between the dipole moment of water molecule and the Z-axis which is shown in Fig. S2 in SI, and $\langle\rangle$ represents the ensemble average. When all water molecules are perpendicular to the pore surface, $S(Z) = 1$; if they are parallel to the pore surface, $S(Z) = -0.5$; $S(Z) = 0$ represents a random orientation. It shows that the water molecules close to the pore surface tend to have their dipole moments parallel to the pore surface, while a random distribution is observed in the middle of the pores, which is in line with Striolo et al. (2003). Based on the water density distributions, we define the interface water region (IWR) which is from the pore surface ($Z = 0$ nm) to the first saddle point in O_w density distributions (Z = 0.50 nm for both DCHA and DHA cases). Most of the hydrophobic tails of NAs are within the IWR due to the hydrophobic interactions and their aggregation at the pore surface as shown in Fig. 4, while DHA molecules are more tightly attached to the pore surface than DCHA molecules. The peak positions in C1 to C7 distributions gradually shift from the pore surface to the middle of the pores. On the other hand, O1 is mostly outside of the IWR to be better hydrated by water or form pairing with Na^+ ions as shown in Fig. 3. However, due to the stronger hydrophobic interactions between DHA and pore surface than those between DCHA and pore surface, the peak value in the O1

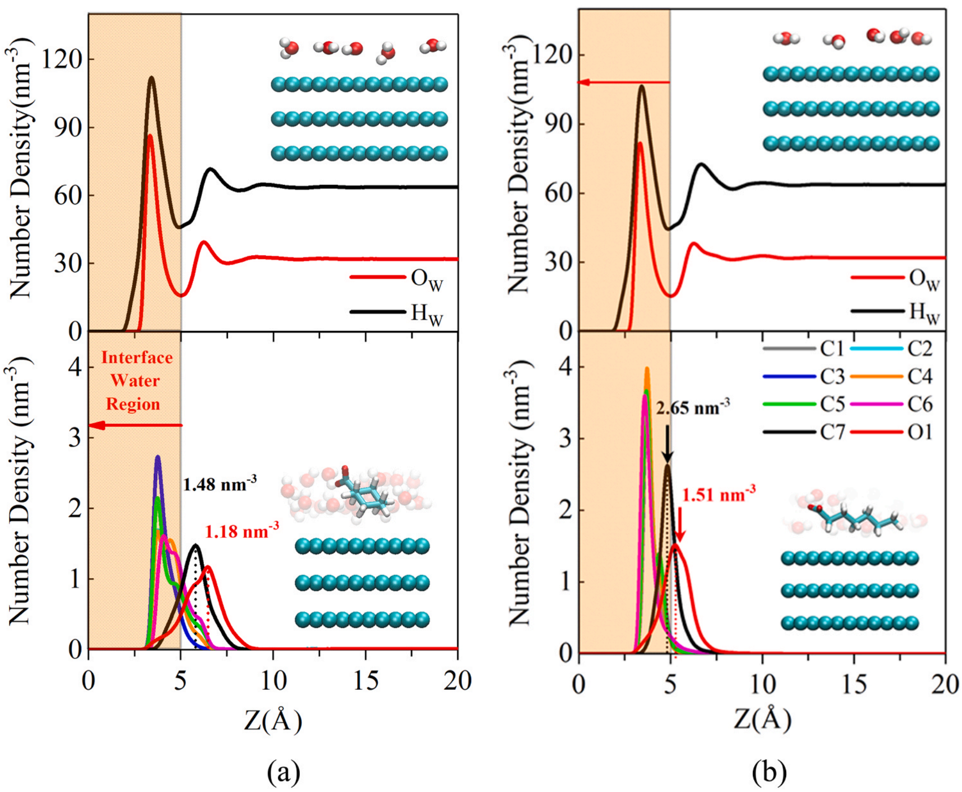

Fig. 5. Number density distributions of each specie in (a) DCHA; (b) DHA and O_W as well as H_w in pristine carbon mesopores. We also present the typical water and NAs configurations within IWR. The specie labels can be found in Fig. 1.

distributions of DHA is higher than that in the O1 distributions of DCHA, and closer to the pore surface as well. For comparison, we also present the number density distributions of each species in NAs and O_W as well as H_W in pristine AC micropores in Fig. S3 in SI. Similar to the pristine AC mesopores, most of the hydrophobic tails of NAs are within the IWR. However, as W decreases, due to the stronger confinement effect, the peak values of O1 and C7 distributions of DCHA increases, while those of DHA remain almost unchanged.

To better assess NAs and water distributions in PACNs, in Fig. S4 in SI, we present the center of mass distributions of DHA and DCHA molecules as well as O_W in pristine AC micropores and mesopores. Based on their center of mass distributions, the number of NAs falling within IWR can be calculated by integrating from $Z = 0$ nm to the first saddle point in O_W density distributions as listed in Table S5. Most of the DHA molecules are within the IWR, while almost half of the DCHA molecules are distributed outside the IWR due to their tilt configurations as shown in Fig. 3. The peak value in DHA center of mass distributions is higher than that of DCHA, while it is closer to the pore surface as well. In addition, the first peak in O_W distributions in the presence of DHA is slightly lower than that of DCHA, suggesting that more water molecules are depleted from the pore surface in the presence of DHA due to stronger hydrophobic interactions.

We also use DCHA and DHA hydrophobic tail orientations to describe their distinct configurations in PACNs, which can be represented by angle probability distribution $P_{angle}(\theta)$ (Skipper et al., 1995),

$$P_{angle}(\theta) = \frac{\sum_{m=1}^{m=k} n(\theta)}{N \times \mathrm{k}} \tag{2}$$

where $n(\theta)$ is the number of NA molecules with their angles in the range from θ to $\theta + d\theta$, N is the total number of NA molecules, k is the total sampling frames. We define the angle θ between the vector from C1 to C6 and the Z-direction for DHA molecules. For DCHA molecules, it is defined as the angle between the normal vector of a plane consisting of three ring carbons (C2-C4-C6) and the X-direction. $\theta = 0^\circ$ and $\theta = 90^\circ$ represent perpendicular and parallel orientation to the surface, respectively. The angle definitions for NAs are shown in Fig. S5. $P_{angle}(\theta)$ of DCHA and DHA in PACNs are presented in Fig. S6. For DHA, $P_{angle}(\theta)$ has a strong peak at 90°, which corresponds to a parallel orientation to the pore surface. In contrast, $P_{angle}(\theta)$ for DCHA has a broader distribution with a smaller peak value at 90°, indicating that the parallel orientation is less obvious.

3.2. HACNs

In Fig. 6, we present the schematic representations of the equilibrated systems with DCHA and DHA, Na^+ ions as well as water molecules in HACNs. In contrast to PACNs, due to the presence of -OH groups on the pore surface, the hydrophobic interactions between NAs and pore surface are greatly reduced. Both NAs tend to align their hydrophilic heads toward the -OH groups via hydrogen bonding with their hydrophobic tails extending into the middle of the pores. As a result, the hydrophobic tails of NAs are no longer parallel to the pore surface, but more perpendicular to the pore surface. Such phenomenon is also observed for decanoic acids near kaolinite surface (Underwood et al., 2016). Similar to PACNs, the Na^+ ions are depleted from the pore surface.

The aerial views of the X-Y plane with DHA and DCHA in hydroxylated AC mesopores are displayed in Fig. 7. For DCHA, the plane view covers the region from $Z = 0$ to $Z = 0.8$ nm, while for DHA, it covers the region from $Z = 0$ to $Z = 1.2$ nm. $Z = 0.8$ nm for DCHA and $Z = 1.2$ nm for DHA correspond to the positions where the C3 and C1 number density is close to 0, respectively, as shown in Fig. 8. In contrast to Fig. 4, in HACNs, DHA and DCHA are adsorbed on the pore surface via the H-bond with -OH groups aligning perpendicular to the pore surface. While both DHA and DCHA can aggregate in PACNs as shown in Fig. 4, both of

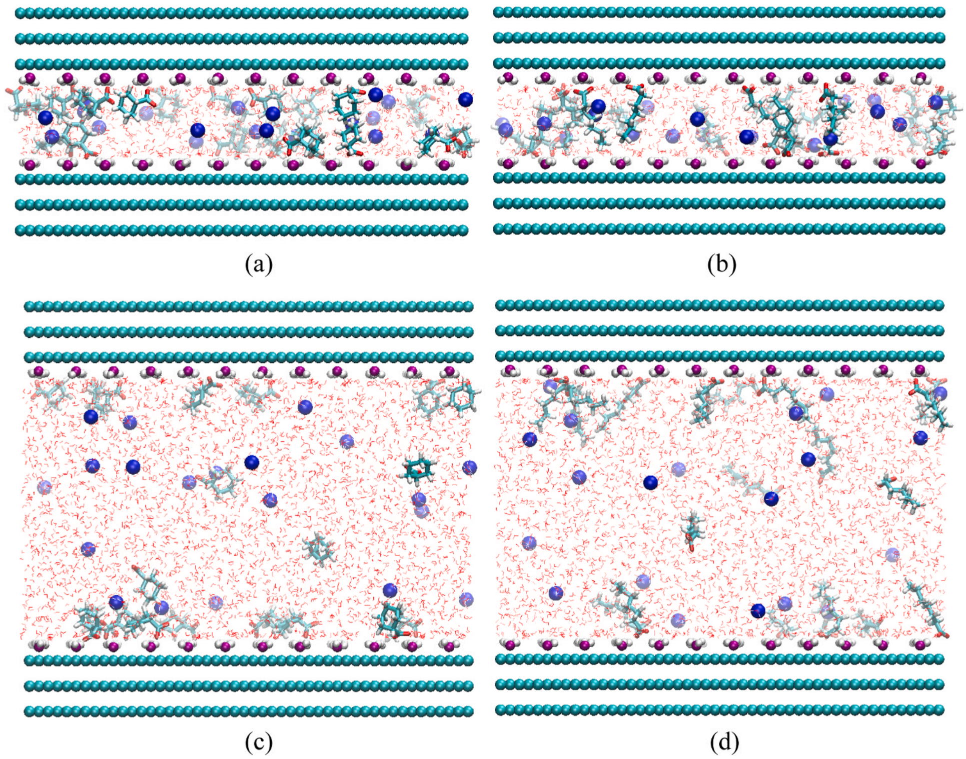

Fig. 6. Schematic representations of (a) DCHA; (b) DHA, Na^+ ions, and water molecules in hydroxylated AC micropores and (c) DCHA; (d) DHA, Na^+ ions, and water molecules in hydroxylated AC mesopores. Color scheme: white, H; purple, O of -OH groups; red, O of water and NAs; blue, Na^+. For clarity, water molecules are presented by the line mode. (For interpretation of the references to color in this figure legend, the reader is referred to the web version of this article.)

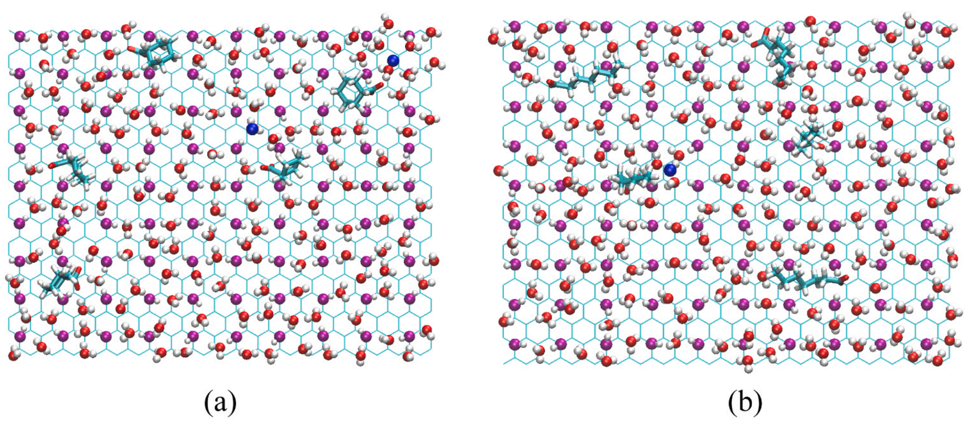

Fig. 7. The aerial view of the *X-Y* plane with (a) DCHA; (b) DHA in pristine AC mesopores. For DCHA, the plane view covers the region from $Z = 0$ to $Z = 0.8$ nm; For DHA, the plane view covers the region from $Z = 0$ to $Z = 1.2$ nm.

them are well dispersed in HACNs. Water forms strong clustering around -OH groups via the H-bond, and NAs can also form the H-bond with -OH groups by depleting a small number of water molecules. However, in contrast to Fig. 4, the water depletion is less obvious. The predominant interface water forms a strong film covering the pore surface and preventing the hydrophobic interactions between NAs and the pore surface in HACNs.

In Fig. 8, we depict the number density distributions of each species in NAs and O_w as well as H_w in hydroxylated AC mesopores. In HACNs, due to the hydrogen bonding between water and -OH groups, while O_w has a strong adsorption layer on the pore surface, H_w has a bimodal distribution close to the pore surface, indicating a non-parallel orientation of water molecules in the vicinity of the pore surface in line with their configurations shown in Fig. 8. As shown in Fig. S7, $S(Z)$ of water molecules also indicate that water molecules adopt more perpendicular orientations comparing to those in PACNs. In HACNs, the IWR is defined as the region from the pore surface ($Z = 0$ nm) to the first saddle point in the O_w density distributions ($Z = 0.45$ nm for both DCHA and DHA cases). The thickness of IWR in HACNs is smaller than that in PACNs due to a more packed water distribution thanks to the H-bonds with -OH groups. In contrast to Fig. 5, the hydrophobic tails of NAs are largely located outside the IWR, while only the hydrophilic heads are within the IWR. O1 has a strong adsorption on the pore surface, while C7 has a bimodal distribution within the IWR. For DCHA, the first peak in the bimodal C7 distribution is lower than the second peak, while for DHA, the two peaks are comparable. The bimodal C7 distribution is probably due to the NA orientations close to the pore surface, as they can align O1-O2 vector either parallel to the surface (standing on the surface) or perpendicular to the surface (resting on the surface) as shown in Fig. S8. While DCHA prefers the standing configuration, DHA have

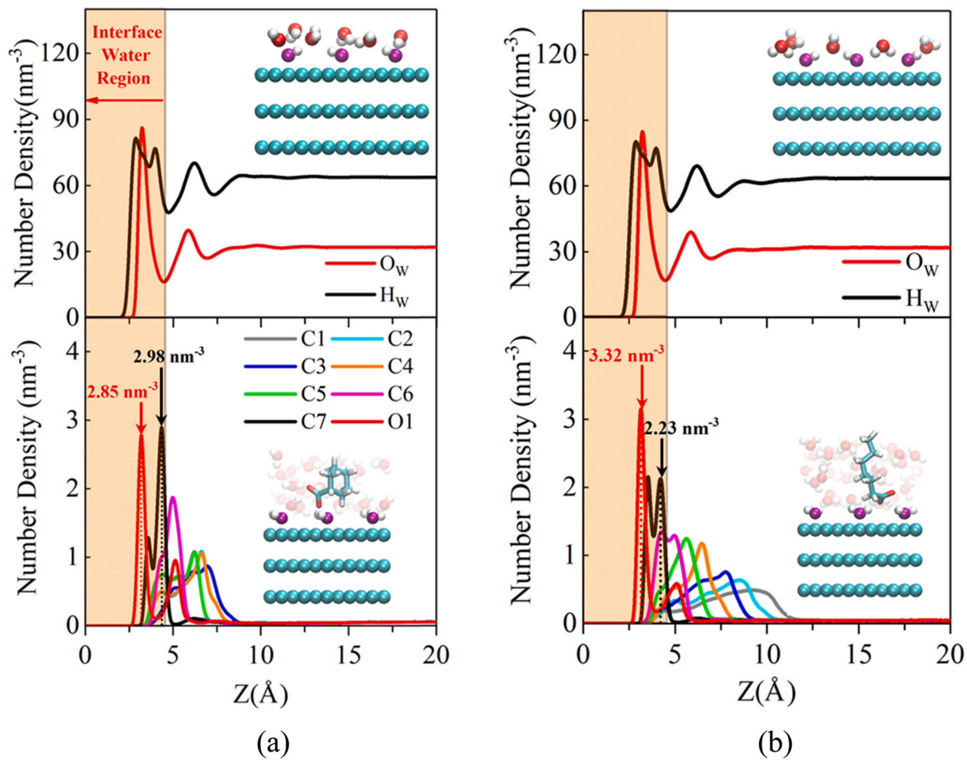

Fig. 8. Number density distributions of each specie in (a) DCHA; (b) DHA and O_w as well as H_w in hydroxylated AC mesopores. We also present the water and NAs orientations within IWR. The specie labels can be found in Fig. 1.

approximately equal probability of the standing and resting configurations. Similar phenomena are also observed for micropores, while the peak value in the O1 distributions increases slightly due to the confinement effect, as depicted in Fig. S9.

To better understand water distributions close to the pore surface, in Fig. S10, we present 2-D density contour plots of O_w in its first adsorption layer, which is defined as the region from the first non-zero density to the first local minimum in O_w distributions as shown in Fig. 8. The blue spots in Fig. S10 correspond to the locations of -OH groups. It shows that water molecules form clustering around the -OH groups through H-bonding. To better illustrate this phenomenon, the radial density distribution (RDD) of O_w, O1 in NAs, and Na^+ ions around H atoms of -OH groups (H_{OH}) in hydroxylated AC mesopores is displayed in Fig. 9. A strong first peak in O_w distributions around H_{OH} indicates the water clustering around the -OH groups. On the other hand, O1 distributions also show an adsorption around H_{OH}, corresponding to the H-bond as shown in Fig. 7. Na^+ ions are generally depleted from the -OH groups. Thanks to the H-bond between NAs and -OH groups, the hydration and Na^+ pairing number of O1 atom in HACNs are much lower than those in PACNs, as shown in Table S3.

We also present the average hydrogen bond number per -OH group between water and -OH groups and between NAs and -OH groups in HACNs in Table S4. The hydrogen bonds are identified based on a geometrical criterion, in which a hydrogen bond is determined (Kumar et al., 2007) if $r\mathrm{O}\cdots\mathrm{O} < 3.5$ Å and $\angle \mathrm{O}\cdots\mathrm{O{-}H} \leq 30°$. Each -OH group forms close to two hydrogen bonds with water molecules. Therefore, water clustering around -OH groups are greatly promoted, which negatively affect the hydrophobic interactions between NAs and the pore surface. In contrast, -OH groups can form much fewer hydrogen bonds with NAs. The hydrogen bond number between NAs and -OH groups in mesopores is slightly lower than that in micropores because some NA molecules are distributed in the middle of the pore in

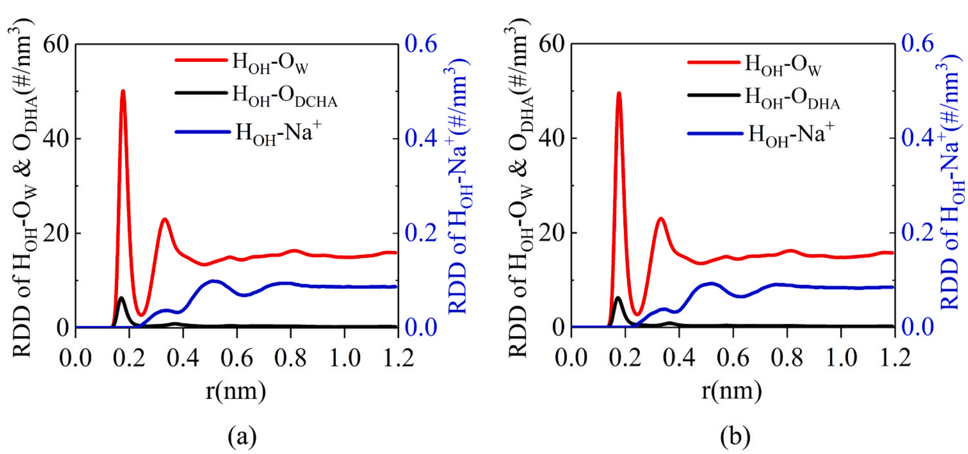

Fig. 9. Radial distribution density for O_w, O1 in NAs, and Na^+ ions around H_{OH} in the presence of (a) DCHA; (b) DHA for hydroxylated AC mesopores.

mesopores. To better display the hydrogen bonds, the hydrogen bond networks in hydroxylated AC micropores are shown in Fig. S11. Generally, most -OH groups can interact with two water molecules via hydrogen bonding. In addition, water molecules can also form hydrogen bonding with each other to form water clusters, which is detrimental to the hydrophobic interactions. Nevertheless, each -OH group can only interact with one NA molecule. It is probably because the net negative charge of NAs can effectively repel each other. As a result, some NAs are no longer tightly attached to the surface and dispersed in the middle of hydroxylated AC mesopores as shown in Fig. 6 (c) and (d). The distinct structural properties of NAs in PACNs and HACNs can probably explain why the O-containing functional groups are detrimental to NA adsorption from water in ACs as observed in experimental measurements (El-Sayed and Bandosz, 2003). To better illustrate the effect of -OH groups on interface water and NA structures, in Fig. S12, we present the center of mass distributions of DHA and DCHA molecules as well as O_w in hydroxylated AC micropores and mesopores. The number of NAs distributed within the IWR is shown in Table S6. In contrast to Fig. S4, both DCHA and DHA molecules are depleted from the IWR, demonstrating a strong interface water structure. The different center of mass distributions of DHA and DCHA are also attributed to the different NA orientations in HACNs, as shown in Fig. S13 (the angle definitions given in Fig. S14). In contrast to PACNs, $P_{angle}(\theta)$ in HACNs no longer concentrates at $\sim 90^{\circ}$, especially for DHA. In HACNs, DCHA displays a peak at $\sim 60^{\circ}$ and $\sim 120^{\circ}$ indicating an inclining orientation of its ring structure, while a broader range distribution from 30° to 150° is observed for DHA suggesting a random configuration.

We note that the current molecular models and simulation approaches applied in this work cannot account for the (-)CAHB between the negatively charged NAs and a negatively-charged carbonaceous surface which has been reported as one of the main driving forces for the adsorption of weak acids on negatively charged carbonaceous surfaces (Moustafa et al., 2014; Li et al., 2015, 2013). The hydrogen bonding between NAs and -OH groups on the carbon surface revealed in this work rather refers to an ordinary one (Gilli et al., 2009), while (-)CAHB is a subset of the low barrier H-bond (Li et al., 2013). Li et al. (2013) studied the pH-dependent adsorption of benzoic acid, phthalic acid, and 2,6-dichloro-4-nitrophenol by hydroxylated, carboxylated, and graphitized carbon nanotubes (CNTs). They observed that their adsorption capacities in various CNTs are higher at pH 2.0 than those at pH 7.0, underscoring the significance of hydrophobic interactions. In addition, at pH 7.0, their adsorption capacities in different CNTs are comparable, demonstrating the important role of the (-)CAHB in weak acid adsorption onto O-containing carbonaceous surfaces. Moustafa et al. (2014) investigated adsorption of ionized weak acids (including decanoic acid, trans-4-isopropyl cyclohexanoic acid, trans-4-propyl cyclohexanoic acid, heptanoic acid, and cyclohexanoic acid) on functionalized expanded graphite (EG) containing phenolic and carboxyl groups from macroscopic thermodynamic perspectives. They compared the solvation free energy of acids in aqueous solution ΔG_{sol}, the free energy of water adsorption to functional groups $\Delta G^{HB}_{H_2O}$, and the free energy of (-)CAHB formation ΔG^{-CAHB}. They argued that ΔG^{-CAHB} needs to overcome $\Delta G^{HB}_{H_2O}$ and ΔG_{sol} (i.e., $\Delta G^{-CAHB} > \Delta G_{sol} > \Delta G^{HB}_{H_2O}$) so that the formation of (-)CAHB between weak acids and carbonaceous surface is probable. As there was no adsorption observed for heptanoic acid and cyclohexanoic acid, they postulated that ΔG^{-CAHB} cannot overcome ΔG_{sol} for these NAs. On the other hand, they observed a noticeable adsorption for decanoic acid with a seemingly similar ΔG^{-CAHB} value (Moustafa et al., 2014). They argued that the increase in the hydrophobicity of NAs due to proton exchange of the deprotonated NA with water can contribute to the energy gain required for (-)CAHB formation (Li et al., 2013; Teixidó et al., 2011). However, we note that decanoic acid has a longer hydrophobic tail than heptanoic acid and cyclohexanoic acid so that its hydrophobic interactions with carbon surface should be more prominent as highlighted in Fig. 3. While the used EG contains phenolic and carboxyl groups, its wettability was not fully characterized. In addition, the applied macroscopic thermodynamic models do not take into account the solute hydration structures in the vicinity of pore surface (the solvation free energy refers to that in the bulk aqueous solutions) nor the interface water structures which can influence the interactions between NAs and surface functional groups. When it comes to the determination of (-)CAHB between weak acids and carbonaceous surfaces, the local solute hydration structures and interface water structures should be fully considered (Zhu et al., 2005). While our molecular models and simulations cannot explicitly take into account the formation of (-)CAHB, our results endorse its potential formation from atomistic and molecular perspectives as even though water forms strong clustering, the deprotonated NAs can form an ordinary H-bond with surface functional groups. The collaborative effect of local solute hydration structures, interface water structures, and the formation of (-)CAHB on weak acid adsorption on carbonaceous surface should be addressed in a multi-scale quantum mechanics/molecular mechanics approach (Warshel and Levitt, 1976) which can be computationally expensive. In addition, carboxylate group is another typical O-containing group with a low pKa value (~ 5) which can lead to negatively charged surfaces due to the deprotonation process. In this case, the electrostatic repulsion between both negatively charged NAs and pore surface, and the formation of (-)CAHB influenced by the local solute hydration structures as well as interface water structures play an important role in NA adsorption from water in AC nanopores.

4. Conclusion

In this work, we use MD simulations to explore the structural properties of NAs and interface water structures in PACNs and HACNs. It is found that the carbon surface properties play an important role in the interface water structures which can in turn greatly influence solute-surface interactions as well as solute configurations.

In PACNs, NAs can aggregate close to the pore surface with their hydrophobic tails attached to the pore surface and hydrophilic heads extending to the middle of the pores, while water molecules can only accumulate on the pore surface where there is no DHA/DCHA aggregation. The hydrophobic tails of NAs are generally within the IWR thanks to strong hydrophobic interactions. In addition, a stronger affinity between the linear carbon tails of DHA and carbon surface is observed comparing to the ring structure of DCHA, which can potentially explain their distinct removal behaviors (Zubot et al., 2012; Quinlan and Tam, 2015).

In HACNs, a predominant interface water layer is formed on the pore surface thanks to the H-bond between water and -OH groups, while both DHA and DCHA molecules are repelled from the pore surface and outside the IWR. Water can form strong clustering around the surface -OH groups and create a water film on the pore surface greatly reducing the hydrophobic interactions between NAs and the pore surface as well as negatively affecting the ordinary H-bond between NAs and -OH groups, which collectively might be detrimental to the NA adsorption from water in ACs. From this perspective, it is suggested that the surface -OH groups should be minimized before the ACs are applied for contaminant remediation.

However, in this work, we did not directly study the adsorption capacity of NAs from water in AC nanopores and the formation of (-)CAHB between the deprotonated NAs and negatively charged carbonaceous surface is not considered in this work (Moustafa et al., 2014; Li et al., 2013), which will be addressed in our future works. In addition, OSPW can contain various salt ions, including Na^+, Ca^{2+}, Mg^{2+}, Cl^-, and SO_4^{2-}, etc. Saidi-Mehrabad et al. (2013). It has been reported that divalent cations can form ion bridging between acids and a negatively charged surface (Yang et al., 2016; Mugele et al., 2016). While some works (Li et al., 2013; Ni et al., 2011; Zhang et al., 2010) have reported that the cation bridging has a negligible effect on weak acid adsorption on carbonaceous surfaces, it is worthwhile to investigate its probability from atomistic and molecular perspectives.

CRediT authorship contribution statement

Mingshan Zhang: Methodology, Software, Validation, Formal analysis, Investigation, Writing - original draft, Writing - review & editing, Visualization. **Wenhui Li**: Methodology, Software, Validation, Writing - review & editing, Visualization. **Zhehui Jin**: Conceptualization, Formal analysis, Investigation, Resources, Writing - review & editing, Supervision, Funding acquisition.

Declaration of Competing Interest

The authors declare that they have no known competing financial interests or personal relationships that could have appeared to influence the work reported in this paper.

Acknowledgement

The authors acknowledge China Scholarship Council (CSC) for financial support provided to M. Zhang and W. Li. This research was enabled in part by support provided by Westgrid (www.westgrid.ca) and Compute Canada (www.computecanada.ca). The authors also greatly acknowledge a Discovery Grant from Natural Sciences and Engineering Research Council of Canada (NSERC RGPIN-2017-05080).

Appendix A. Supporting information

Supplementary data associated with this article can be found in the online version at doi:10.1016/j.jhazmat.2021.125660.

References

A.E. Regulator, 2018. ST98: 2018 Alberta's Energy Reserves & Supply/Demand outlook, Alberta Energy Regulator, Calgary, AB, Canada. Accessed 21 October 2018.
Alam, M.S., Cossio, M., Robinson, L., Wang, X., Kenney, J.P., Konhauser, K.O., MacKenzie, M.D., Ok, Y.S., Alessi, D.S., 2016. Removal of organic acids from water using biochar and petroleum coke. Environ. Technol. Innov. 6, 141–151.
Alejandre, J., Tildesley, D.J., Chapela, G.A., 1995. Molecular dynamics simulation of the orthobaric densities and surface tension of water. J. Chem. Phys. 102, 4574–4583.
Ali, A., Le, T.T.B., Striolo, A., Cole, D.R., 2020. Salt effects on the structure and dynamics of interfacial water on calcite probed by equilibrium molecular dynamics simulations. J. Phys. Chem. C 124, 24822–24836.
Allen, E.W., 2008. Process water treatment in Canada's oil sands industry: I. Target pollutants and treatment objectives. J. Environ. Eng. Sci. 7, 123–138.
Allen, S., Whitten, L., McKay, G., 1998. The production and characterisation of activated carbons: a review. Dev. Chem. Eng. Miner. Process. 6, 231–261.
Bhuiyan, T.I., Tak, J.K., Sessarego, S., Harfield, D., Hill, J.M., 2017. Adsorption of acid-extractable organics from oil sands process-affected water onto biomass-based biochar: metal content matters. Chemosphere 168, 1337–1344.
Choma, J., Jaroniec, M., 2006. Characterization of nanoporous carbons by using gas adsorption isotherms. In: Interface Science and Technology. Elsevier, pp. 107–158.
da Silva, A.H., Miranda, E.A., 2013. Adsorption/desorption of organic acids onto different adsorbents for their recovery from fermentation broths. J. Chem. Eng. Data 58, 1454–1463.
El-Din, M.G., Fu, H., Wang, N., Chelme-Ayala, P., Pérez-Estrada, L., Drzewicz, P., Martin, J.W., Zubot, W., Smith, D.W., 2011. Naphthenic acids speciation and removal during petroleum-coke adsorption and ozonation of oil sands process-affected water. Sci. Total Environ. 409, 5119–5125.
El-Sayed, Y., Bandosz, T.J., 2003. Effect of increased basicity of activated carbon surface on valeric acid adsorption from aqueous solution activated carbon. Phys. Chem. Chem. Phys. 5, 4892–4898.
El-Sayed, Y., Bandosz, T.J., 2004. Adsorption of valeric acid from aqueous solution onto activated carbons: role of surface basic sites. J. Colloid Interface Sci. 273, 64–72.
Figueiredo, J.L., Pereira, M., Freitas, M., Orfao, J., 1999. Modification of the surface chemistry of activated carbons. Carbon 37, 1379–1389.
Frank, R.A., Kavanagh, R., Burnison, B.K., Arsenault, G., Headley, J.V., Peru, K.M., Van Der Kraak, G., Solomon, K.R., 2008. Toxicity assessment of collected fractions from an extracted naphthenic acid mixture. Chemosphere 72, 1309–1314.
Gilli, P., Pretto, L., Bertolasi, V., Gilli, G., 2009. Predicting hydrogen-bond strengths from acid−base molecular properties. The pKa slide rule: toward the solution of a long-lasting problem. Acc. Chem. Res. 42, 33–44.
Immaraporn, B., Ye, P., Gellman, A.J., 2004. The transition state for carboxylic acid deprotonation on Cu (100). J. Phys. Chem. B 108, 3504–3511.
Islam, M.S., Zhang, Y., McPhedran, K.N., Liu, Y., El-Din, M.G., 2015. Granular activated carbon for simultaneous adsorption and biodegradation of toxic oil sands process-affected water organic compounds. J. Environ. Manag. 152, 49–57.
Islam, M.S., McPhedran, K.N., Messele, S.A., Liu, Y., El-Din, M.G., 2018. Isotherm and kinetic studies on adsorption of oil sands process-affected water organic compounds using granular activated carbon. Chemosphere 202, 716–725.
Kozbial, A., Zhou, F., Li, Z., Liu, H., Li, L., 2016. Are graphitic surfaces hydrophobic? Acc. Chem. Res. 49, 2765–2773.
Kumar, R., Schmidt, J., Skinner, J., 2007. Hydrogen bonding definitions and dynamics in liquid water. J. Chem. Phys. 126, 204107.
Li, W., Nan, Y., Zhang, Z., You, Q., Jin, Z., 2020. Hydrophilicity/hydrophobicity driven CO_2 solubility in kaolinite nanopores in relation to carbon sequestration. Chem. Eng. J. 398, 125449.
Li, X., Pignatello, J.J., Wang, Y., Xing, B., 2013. New insight into adsorption mechanism of ionizable compounds on carbon nanotubes. Environ. Sci. Technol. 47, 8334–8341.
Li, X., Gámiz, B., Wang, Y., Pignatello, J.J., Xing, B., 2015. Competitive sorption used to probe strong hydrogen bonding sites for weak organic acids on carbon nanotubes. Environ. Sci. Technol. 49, 1409–1417.
Ma, L., Chen, X., 2016. Adsorption of naphthenic acids to the nitrogen-coordinated transition-metal embedded graphene: a DFT study. Russ. J. Phys. Chem. B 10, 1027–1031.
Moustafa, A.M., McPhedran, K.N., Moreira, Js, Gamal El-Din, M., 2014. Investigation of mono/competitive adsorption of environmentally relevant ionized weak acids on graphite: impact of molecular properties and thermodynamics. Environ. Sci. Technol. 48, 14472–14480.
Mugele, F., Siretanu, I., Kumar, N., Bera, B., Wang, L., de Ruiter, R., Maestro, A., Duits, M., van den Ende, D., Collins, I., 2016. Insights from ion adsorption and contact-angle alteration at mineral surfaces for low-salinity waterflooding. SPE J. 21, 1,204–201,213.
Müller, E.A., Gubbins, K.E., 1998. Molecular simulation study of hydrophilic and hydrophobic behavior of activated carbon surfaces. Carbon 36, 1433–1438.
Ni, J., Pignatello, J.J., Xing, B., 2011. Adsorption of aromatic carboxylate ions to black carbon (biochar) is accompanied by proton exchange with water. Environ. Sci. Technol. 45, 9240–9248.
Niasar, H.S., Li, H., Kasanneni, T.V.R., Ray, M.B., Xu, C.C., 2016. Surface amination of activated carbon and petroleum coke for the removal of naphthenic acids and treatment of oil sands process-affected water (OSPW). Chem. Eng. J. 293, 189–199.
Oda, H., Yamashita, A., Minoura, S., Okamoto, M., Morimoto, T., 2006. Modification of the oxygen-containing functional group on activated carbon fiber in electrodes of an electric double-layer capacitor. J. Power Sources 158, 1510–1516.
Orth, E.S., Ferreira, J.G., Fonsaca, J.E., Blaskievicz, S.F., Domingues, S.H., Dasgupta, A., Terrones, M., Zarbin, A.J., 2016. pKa determination of graphene-like materials: validating chemical functionalization. J. Colloid Interface Sci. 467, 239–244.
Pelekani, C., Snoeyink, V., 1999. Competitive adsorption in natural water: role of activated carbon pore size. Water Res. 33, 1209–1219.
Pendleton, P., Wu, S.H., Badalyan, A., 2002. Activated carbon oxygen content influence on water and surfactant adsorption. J. Colloid Interface Sci. 246, 235–240.
Qiao, Z.-A., Wang, Y., Gao, Y., Li, H., Dai, T., Liu, Y., Huo, Q., 2010. Commercially activated carbon as the source for producing multicolor photoluminescent carbon dots by chemical oxidation. Chem. Commun. 46, 8812–8814.
Quinlan, P.J., Tam, K.C., 2015. Water treatment technologies for the remediation of naphthenic acids in oil sands process-affected water. Chem. Eng. J. 279, 696–714.
Quinlivan, P.A., Li, L., Knappe, D.R., 2005. Effects of activated carbon characteristics on the simultaneous adsorption of aqueous organic micropollutants and natural organic matter. Water Res. 39, 1663–1673.
Rouquerol, J., Avnir, D., Fairbridge, C., Everett, D., Haynes, J., Pernicone, N., Ramsay, J., Sing, K., Unger, K., 1994. Recommendations for the characterization of porous solids (Technical Report). Pure Appl. Chem. 66, 1739–1758.
Saidi-Mehrabad, A., He, Z., Tamas, I., Sharp, C.E., Brady, A.L., Rochman, F.F., Bodrossy, L., Abell, G.C., Penner, T., Dong, X., 2013. Methanotrophic bacteria in oilsands tailings ponds of northern Alberta. ISME J. 7, 908–921.
Sing, K.S., 1985. Reporting physisorption data for gas/solid systems with special reference to the determination of surface area and porosity (Recommendations 1984). Pure Appl. Chem. 57, 603–619.
Skipper, N., Sposito, G., Chang, F.-R.C., 1995. Monte Carlo simulation of interlayer molecular structure in swelling clay minerals. 2. Monolayer hydrates. Clays Clay Miner. 43, 294–303.
Slavcheva, E., Shone, B., Turnbull, A., 1999. Review of naphthenic acid corrosion in oilrefining. Br. Corros. J. 34, 125–131.
Spitzer, J.J., Heerze, L.D., 1983. Adsorption of cycloalkane and cyclopentanealkyl acids at the air/water interface. Can. J. Chem. 61, 1067–1070.
Stringham, G., 2012. Energy developments in Canada's oil sands. In: Developments in Environmental Science. Elsevier, pp. 19–34.
Striolo, A., Chialvo, A.A., Cummings, P.T., Gubbins, K.E., 2003. Water adsorption in carbon-slit nanopores. Langmuir 19, 8583–8591.
Teixidó, M., Pignatello, J.J., Beltrán, J.L., Granados, M., Peccia, J., 2011. Speciation of the ionizable antibiotic sulfamethazine on black carbon (biochar). Environ. Sci. Technol. 45, 10020–10027.
Thomas, J.A., McGaughey, A.J.H., 2009. Water flow in carbon nanotubes: transition to subcontinuum transport. Phys. Rev. Lett. 102, 184502.
Ulberg, D.E., Gubbins, K.E., 1995. Water adsorption in microporous graphitic carbons. Mol. Phys. 84, 1139–1153.
Underwood, T., Erastova, V., Greenwell, H.C., 2016. Wetting effects and molecular adsorption at hydrated kaolinite clay mineral surfaces. J. Phys. Chem. C 120, 11433–11449.

Wang, N., Chelme-Ayala, P., Perez-Estrada, L., Garcia-Garcia, E., Pun, J., Martin, J.W., Belosevic, M., Gamal El-Din, M., 2013. Impact of ozonation on naphthenic acids speciation and toxicity of oil sands process-affected water to Vibrio fischeri and mammalian immune system. Environ. Sci. Technol. 47, 6518–6526.

Warshel, A., Levitt, M., 1976. Theoretical studies of enzymic reactions: dielectric, electrostatic and steric stabilization of the carbonium ion in the reaction of lysozyme. J. Mol. Biol. 103, 227–249.

Wu, J., Jiang, T., Jiang, D.-e, Jin, Z., Henderson, D., 2011. A classical density functional theory for interfacial layering of ionic liquids. Soft Matter 7, 11222–11231.

Wu, S.H., Pendleton, P., 2001. Adsorption of anionic surfactant by activated carbon: effect of surface chemistry, ionic strength, and hydrophobicity. J. Colloid Interface Sci. 243, 306–315.

Yang, J., Dong, Z., Dong, M., Yang, Z., Lin, M., Zhang, J., Chen, C., 2016. Wettability alteration during low-salinity waterflooding and the relevance of divalent ions in this process. Energy Fuels 30, 72–79.

Yang, J., Pignatello, J.J., Yang, K., Wu, W., Lu, G., Zhang, L., Yang, C., Dang, Z., 2021. Adsorption of organic compounds by biomass chars: direct role of aromatic condensation (ring cluster size) revealed by experimental and theoretical studies. Environ. Sci. Technol. 55, 1594–1603.

Yuan, M., Tong, S., Zhao, S., Jia, C.Q., 2010. Adsorption of polycyclic aromatic hydrocarbons from water using petroleum coke-derived porous carbon. J. Hazard. Mater. 181, 1115–1120.

Zhang, J., Choi, S., 2006. Molecular dynamics simulation of methane in potassium montmorillonite clay hydrates. J. Phys. B At. Mol. Opt. Phys. 39, 3839–3848.

Zhang, S., Shao, T., Bekaroglu, S.S.K., Karanfil, T., 2010. Adsorption of synthetic organic chemicals by carbon nanotubes: effects of background solution chemistry. Water Res. 44, 2067–2074.

Zhu, D., Kwon, S., Pignatello, J.J., 2005. Adsorption of single-ring organic compounds to wood charcoals prepared under different thermochemical conditions. Environ. Sci. Technol. 39, 3990–3998.

Zhu, S., Wang, P., Yang, X.-b, Jin, C., Qiu, R., 2021. Coupling experiments with calculations to understand the thermodynamics evolution for the sorption of zwitterionic ciprofloxacin on oxidizing-aged pyrogenic chars in the aquatic system. J. Hazard. Mater. 411, 125101.

Zubot, W., MacKinnon, M.D., Chelme-Ayala, P., Smith, D.W., Gamal El-Din, M., 2012. Petroleum coke adsorption as a water management option for oil sands process-affected water. Sci. Total Environ. 427–428, 364–372.